TRUS Image Segmentation Driven by Narrow Band Contrast Pattern Using Shape Space Embedded Level Sets

Pengfei Wu[1], Yiguang Liu[1,⋆], Yongzhong Li[2], and Liping Cao[3]

[1] School of Computer Science, Sichuan University, Chengdu, China
[2] Ultrasound Department of West China Hospital, Sichuan University, Chengdu, China
[3] Library, Sichuan University, Chengdu, China
lygpapers@yahoo.com.cn

Abstract. Prostate segmentation in transrectal ultrasound (TRUS) images is highly desired in many clinical applications. However, manual segmentation is difficult, time consuming and irreproducible. In this paper, we present a novel automatic approach using narrow band contrast pattern to segment prostates in TRUS images. Implicit representation of the segmenting level sets curve is firstly trained via principal component analysis, which also constraints the shape of prostate into a linear subspace. Then the model evolves to segment the prostate by maximizing the contrast in a narrow band near the segmenting curve. Many experimental results demonstrate the performance of the proposed algorithm, whose favorableness is validated by comparing to the state-of-the-art algorithms. Especially, the shape of prostate segmented by our algorithm is close to the one manually obtained by expert, and the mean absolute distance is only 1.07 ± 0.77mm, which is quite promising.

Keywords: Prostate segmentation, transrectal ultrasound images, active contours, level sets, shape prior, narrow band contrast pattern.

1 Introduction

Prostate cancer is one of the major public health problems. It is the second leading cause of cancer death among men, only surpassed by lung cancer [1]. Transrectal ultrasound (TRUS) has been the main imaging modality for prostate related applications for various reasons: It is real-time realization, low cost, simplicity and is not inferior to MRI or CT in terms of diagnostic value. Accurate prostate segmentation is significant in many clinical applications. For example, both biopsy needle placement [2] and the measurement of the prostate gland volume [3] require the segmentation information.

However, accurate computer aided prostate segmentation from TRUS images encounters considerable challenges due to low signal-to-noise ratio (SNR)

⋆ Corresponding author.

J. Yang, F. Fang, and C. Sun (Eds.): IScIDE 2012, LNCS 7751, pp. 339–346, 2013.

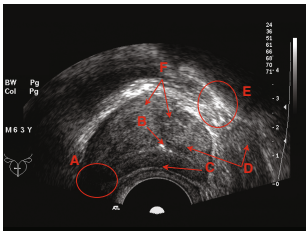

Fig. 1. Challenges for segmentation of prostate boundaries from TRUS images. (A) Shadow artifact and blurred boundary. (B) Area of calcification inside the prostate. (C) Low SNR and contrast. (D) Homogeneity in both prostate and non-prostate tissues. (E) Large speckles. (F) Heterogeneous intensity distribution inside the prostate.

and contrast, speckles, shadow artifact and heterogeneous intensity distribution inside the prostate etc.. Fig. 1 shows an illustration of these challenges. Accordingly, a few prostate segmentation methods have been proposed in literature [4]. Since the inherent difficulties of prostate segmentation in TRUS images, we should take as much prior knowledge, such as prostate shape, as possible into consideration to facilitate the segmentation procedure. As a consequence, statistical shape models gain the most interests and demonstrate a better results of segmentation [5,6,7,8,9]. Zhan et al. [7] used Gabor filter banks to extract texture features in TRUS images, then support vector machines (SVMs) were employed to classify them. After that, the classification result was used to drive the shape model to the prostate boundary. Although this method gains nice experimental results, it is too computational expensive. Yan et al. [6] proposed an automatic method to segment prostate using partial active shape model. Like may other active shape models (ASM) [10] based methods, the evolution of model relies on discrete control points on the model and is prone to be trapped by interferences such as speckles and small areas of calcification. More over, gradient based evolution can't handle the fuzzy edges well, which is often the case in TRUS images due to low SNR and homogeneity of both prostate tissue and non-prostate one.

In this paper, we attempt to create a novel automatic method to address the aforementioned problems. Our method is a level sets approach under the constraint of shape prior. During the segmentation, the model is driven by the proposed narrow band contrast pattern (NBCP) to the prostate boundary. Since the homogeneity of both side of prostate and the majority of useful information is near the prostate boundary, which makes Chan-Vese model [11] impractical, the NBCP only takes information in a narrow band near the model into consideration. At the same time, the NBCP shares part of advantages of Chan-Vese model and don't locally rely on the edge-function, which depends on the gradient of the image, to stop the curve evolution. The proposed model don't require large gradient value near the target boundary and has a large detection range, which is quite important to model initialization. Since our method is a level sets approach, no control points are used and the problem caused by ASM won't rise here. Besides, multi-resolution fashion is utilized to relieve the computational load and enlarge the detection range of the model.

The rest of this paper is organized as follows. How to embed shape prior into level sets is discussed briefly in Section 2. The details of narrow band contrast pattern and the use of it to segment prostate are given in Section 3. Section 4 shows the model initialization method, followed by Section 5 which demonstrates the performance of the proposed method by many experiments. Finally, concluding remarks are drawn in Section 6.

2 Level Sets Embedded with Shape Space

In this section, we briefly discuss the method in [8], which is utilized in our approach for its nice performance and easy to implement feature.

Firstly, a set of training images is segmented manually by expert. Then the segmentation results are aligned to eliminate the influence of different volumes as well as different places of prostate in the TRUS images. The aligned segmentation results are treated as the zero level sets and a set of signed distance functions (SDF) $\{\Psi_i\}$ are constructed from them. After that, mean shape $\bar{\Phi}$ is subtracted from them and they are converted to large column vectors $\{\psi_i\}$. Next, define the shape-variability matrix $\mathcal{S}$ as

$$\mathcal{S} = (\psi_1 \ \psi_2 \ \cdots \ \psi_n) \ . \tag{1}$$

We extract the first k eigenvectors of $\mathcal{S}$ and reshape them to the size the same as the training images. They are represented by $\{\Phi_i\}_{i=1,2,\ldots,k}$. With scale, translation and rotation of the shape taken into account, the implicit description of shape is finally given by the zero level set of the following function:

$$\Phi[\mathbf{w}, \mathbf{p}](x, y) = \bar{\Phi}(\tilde{x}, \tilde{y}) + \sum_{i=1}^{k} \omega_i \Phi_i(\tilde{x}, \tilde{y}) \ , \tag{2}$$

where ω_i is the weight of each eigen-shape Φ_i,

$$\begin{bmatrix} \tilde{x} \\ \tilde{y} \\ 1 \end{bmatrix} = T[\mathbf{p}] \begin{bmatrix} x \\ y \\ 1 \end{bmatrix} \ , \tag{3}$$

$$T[\mathbf{p}] = \begin{bmatrix} h\cos(\theta) & -h\sin(\theta) & a \\ h\sin(\theta) & h\cos(\theta) & b \\ 0 & 0 & 1 \end{bmatrix} \ , \tag{4}$$

and $\mathbf{p} = (a, b, h, \theta)^T$ is the pose parameter.

3 Narrow Band Contrast Pattern

In TRUS images, The prostate boundary has the property of dark-to-light transition of intensities from the inside of the prostate to the outside. However, this property is more notable in upper boundary in most cases. While the left,

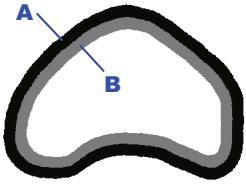

Fig. 2. Narrow band near the model boundary. Black area with label 'A' is outer band satisfying $0 < \Phi \leq h$, while gray area with label 'B' is the inner band satisfying $-h \leq \Phi < 0$.

right and bottom boundaries are significantly blurred, which might lead gradient based segmenting method to failure. Fortunately, the proposed NBCP not only can detect the blurred boundary well, but also is not sensitive to noises, speckles and areas of calcification etc., for its area based property. In this section, we first propose the energy function of NBCP, then the minimal cost approach of our method is discussed in details.

3.1 Energy Function

Because of the property of dark-to-light transition of intensities from the inside of the prostate to the outside, we hope to maximize the intensities in the narrow band outside the prostate boundary while minimize them in the narrow band inside it. So our NBCP energy function is defined as

$$E = -\iint_{\Omega} \tilde{H}(\Phi)I - \tilde{H}(-\Phi)I \,\mathrm{d}A \,, \tag{5}$$

where Ω is the TRUS image, I is the intensity value and Φ is defined previously in (2). The function $\tilde{H}(\cdot)$ makes sure only the pixels in the narrow band of model boundary are taken into account

$$\tilde{H}(\Phi) = \begin{cases} 1, & \text{if } 0 < \Phi \leq h \\ 0, & \text{if } \Phi > h \text{ or } \Phi \leq 0 \end{cases}, \tag{6}$$

where h is a predefined bandwidth value. It's worthy to point out that Φ got in (2) may not be a SDF and the narrow band is not strict h-pixel width. However, during our experiments, this fact doesn't cause any disastrous results. Fig. 2 shows an example of narrow band generated by (6), which is quite acceptable although Φ may not be a strict SDF.

3.2 Minimal Cost Approach

Since Φ is parametrical represented by $\mathbf{w}$ and $\mathbf{p}$, instead of using the Euler-Lagrange equations to do the minimal cost approach of (5), the gradient descent approach is proper here. The gradient of E is given by

$$\begin{aligned}\nabla E &= -\iint_{\Omega} \nabla\tilde{H}(\Phi)I - \nabla\tilde{H}(-\Phi)I \,\mathrm{d}A \\ &= -\iint_{\Omega} \delta(\Phi)\nabla\Phi I - \delta(\Phi - h)\nabla\Phi I \\ &\quad -\delta(-\Phi)\nabla(-\Phi)I + \delta(-\Phi - h)\nabla(-\Phi)I \,\mathrm{d}A \\ &= -2\oint_{\Phi=0} \nabla\Phi I \,\mathrm{d}s + \oint_{\Phi=h} \nabla\Phi I \,\mathrm{d}s + \oint_{\Phi=-h} \nabla\Phi I \,\mathrm{d}s \,, \end{aligned} \tag{7}$$

where $\delta(\cdot)$ is Dirac delta function. The gradient of Φ taken with respect to ω_i is

$$\nabla_{\omega_i}\Phi = \Phi_i \,, \tag{8}$$

while it taken with respect to $\mathbf{p}^i$ (the i-th element of $\mathbf{p}$) by chain rule is

$$\nabla_{\mathbf{p}^i}\Phi = \begin{bmatrix} \dfrac{\partial\Phi}{\partial\tilde{x}} & \dfrac{\partial\Phi}{\partial\tilde{y}} & 0 \end{bmatrix} \frac{\partial T[\mathbf{p}]}{\partial\mathbf{p}^i} \begin{bmatrix} x \\ y \\ 1 \end{bmatrix} \,, \tag{9}$$

where $T[\mathbf{p}]$ is perviously defined in (4).

The segmentation process is implemented by updating the parameter $\mathbf{w}$ and $\mathbf{p}$ based on gradient descent.

4 Initialization

The initialization of the model is a search procedure in the image Ω, by setting $\mathbf{p}$ with different values while $\mathbf{w} = \mathbf{0}$, which implies the mean model $\bar{\Phi}$ is scaled, rotated and translated to different places to find the minimal E using (5). Since the resolution of original TRUS image can be high, the search initialization procedure is performed in the coarsest resolution in our multi-resolution framework to relieve the computational load into a feasible scale. However, because $\mathbf{w}$ is set fixed during the search procedure, the initial model can't fit the target contour exactly. Fortunately, our energy function (5) is quite robust to this coarse fit, for the information in a narrow band near it is taken into account. What's more, for each tentatively set $\mathbf{p}$, a small number of evolution step is performed. Then the energy $E(\mathbf{p})$ is set to the minimal one during this tentative evolution. This procedure further enhance the accuracy of initialization and the problem caused by the fixed model shape is further reduced.

5 Experimental Results and Discussion

Ultrasound images used in the experiments were obtained by using a Philips HDI 5000 sonographic imaging system. Each image has 576×768 pixels. The pixel sizes of the images are 0.1384×0.1384mm. The settings of the device to acquire different images were the same. In our experiments, totally 132 TRUS images were segmented by one expert, 47 of them were used to train the model, while

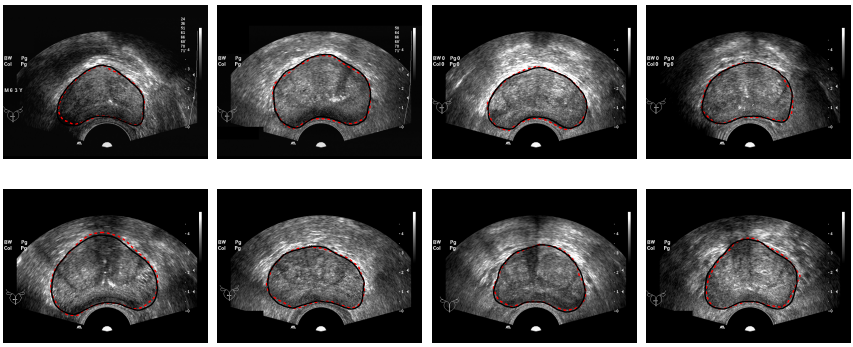

Fig. 3. Some segmentation results. Solid lines are the prostates segmented by the proposed algorithm, while the dash lines represent the contours segmented by expert.

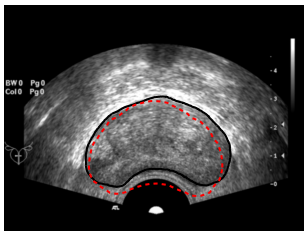

Fig. 4. Example of initialization, with initial model shown in dashes line, while the final segmentation result shown in solid line

the rest 85 ones were used to validate the algorithm. What's more, each slice was processed for individual patient and the consent of all patients was obtained for this study. Our method was implemented in Matlab on a notebook computer with Intel 2.4 Ghz processor. The mean processing time during our experiments of the entire method is about 17s with Matlab scripts. We are hoping to segment one TRUS image in seconds by fully optimizing the code and implementing it in C++ in the near future.

In order to evaluate the efficiency and robustness of our algorithm, distance and area criteria were used by comparing the automatic segmentation result with the segmentation made by the expert. For distance-based metric, the mean absolute distance (MAD) error [6] was utilized. For area-based metric, the coverage (Cov) [12] was employed.

In our experiments, the predefined bandwidth h is set to 20 pixels in the original image and the multi-resolution framework has 4 levels. First, the experiments were done to validate the effectiveness of our initialization algorithm. During our experiments, all the initial model were located in acceptable places. It's worthy to point out that the initial model is by no means to be accurate enough, for the variance of prostate shape while the shape parameter $\mathbf{w}$ is set to be fixed. However, the multi-resolution framework as long as the property of our energy function to consider the information around the boundary of model

Table 1. Prostate Segmentation Evaluation

Method	MAD	Cov
S. Ghose [5]	1.50±0.41mm	-
Yan [6]	2.01±1.02mm	-
N. Betrouni [12]	2.5±0.9mm	93±9%
Cosío [13]	1.65±0.67mm	-
Our Method	1.07±0.77mm	90±7%

enable our algorithm to have a large detection range to the target contour. Fig. 4 shows an example of initial model in dashes line and the final result in solid line. Because of the difference between the mean shape and the target prostate, the initial model didn't fit the target well. But our algorithm still got a good result.

Then experiments were done to segment the set of real TRUS images mentioned above. Some example segmentation results with many challenges mentioned previously to show the robustness of our algorithm is illustrated in Fig. 3, which are compared with the 'golden truth' given by the expert. Table 1 shows the quantitative evaluation results of the our automatic segmentation method, with a compare with some other state-of-the-art algorithms. The symbol '-' in Table 1 means not given. From the table we can see that our experimental results are quite inspiring, because of the small MAD error we got. Note that our method doesn't need any preprocess or postprocess procedure. The performance of our method can be further improved by adopting some postprocess methods, such as active contour model [14] used in [6]. Compared with the small mean value of MAD we got, the standard deviation seems large. The reason is that each slice used to validated our algorithm was obtained from individual patient. As a consequence, the TRUS images varied a lot and so many tough situations rose. While many other algorithms were only validated by limited number of data sets (e.g. [5,6]), though the number of images may be large.

6 Conclusions

In this paper, we have introduced a novel automatic approach using narrow band contrast pattern to segment prostates in TRUS images. Implicit representation of the segmenting level sets curve is firstly trained via principal component analysis, which also constraints the shape of prostate into a linear subspace. Then the model tries to maximize the contrast in a narrow band near the segmenting curve and drives the curve to prostate contour. The algorithm is robust to blurred boundary, low SNR, speckles and calcification, and the performance of it is validated by many experimental results. For example, the shape of prostate segmented by our algorithm is close to the one manually obtained by expert; the mean absolute distance is only 1.07 ± 0.77mm. All the results imply that our algorithm is quite promising.

Acknowledgement. This work is supported by NSFC under grants 61173182 and 61179071, as well as by Applied Basic Research Project (2011JY0124), International Cooperation and Exchange Project (2012HH0004) of Sichuan Province.

References

1. American Cancer Society: The prostate cancer quandary (2011), http://www.cancer.org/
2. Shen, D., Lao, Z., Zeng, J., Zhang, W., Sesterhenn, I.A., Sun, L., Moul, J.W., Herskovits, E.H., Fichtinger, G., Davatzikos, C.: Optimized prostate biopsy via a statistical atlas of cancer spatial distribution. Med. Image Anal. 8(2), 139–150 (2004)
3. Terris, M., Stamey, T.: Determination of prostate volume by transrectal ultrasound. J. Urol. 145(5), 984 (1991)
4. Noble, J.A., Boukerroui, D.: Ultrasound image segmentation: a survey. IEEE Trans. Med. Imag. 25(8), 987–1010 (2006)
5. Ghose, S., Oliver, A., Martí, R., Lladó, X., Freixenet, J., Villanova, J., Meriaudeau, F.: Prostate segmentation with local binary patterns guided active appearance models. Medical Imaging: Image Processing, France (2011)
6. Yan, P., Xu, S., Turkbey, B., Kruecker, J.: Discrete deformable model guided by partial active shape model for trus image segmentation. IEEE Trans. Biomed. Eng. 57(5), 1158–1166 (2010)
7. Zhan, Y.Q., Shen, D.G.: Deformable segmentation of 3-d ultrasound prostate images using statistical texture matching method. IEEE Trans. Med. Imag. 25(3), 256–272 (2006)
8. Tsai, A., Yezzi Jr., A., Wells, W., Tempany, C., Tucker, D., Fan, A., Grimson, W.E., Willsky, A.: A shape-based approach to the segmentation of medical imagery using level sets. IEEE Trans. Med. Imag. 22(2), 137–154 (2003)
9. Shen, D.G., Zhan, Y.Q., Davatzikos, C.: Segmentation of prostate boundaries from ultrasound images using statistical shape model. IEEE Trans. Med. Imag. 22(4), 539–551 (2003)
10. Cootes, T.F., Taylor, C.J., Cooper, D.H., Graham, J.: Active shape models-their training and application. Comput. Vis. Image Understanding 61(1), 38–59 (1995)
11. Chan, T., Vese, L.A.: An Active Contour Model without Edges. In: Nielsen, M., Johansen, P., Fogh Olsen, O., Weickert, J. (eds.) Scale-Space 1999. LNCS, vol. 1682, pp. 141–151. Springer, Heidelberg (1999)
12. Betrouni, N., Vermandel, M., Pasquier, D., Maouche, S., Rousseau, J.: Segmentation of abdominal ultrasound images of the prostate using a priori information and an adapted noise filter. Compt. Med. Imag. and Graph. 29, 43–51 (2005)
13. Cosío, F.A.: Automatic initialization of an active shape model of the prostate. Med. Image Anal. 12(4), 469–483 (2008)
14. Kass, M., Witkin, A., Terzopoulos, D.: Snakes: Active contour models. Int. J. Comput. Vis. 1(4), 321–331 (1988)